IEEE Access
Multidisciplinary ⋮ Rapid Review ⋮ Open Access Journal

Received 18 October 2023, accepted 20 November 2023, date of publication 23 November 2023,
date of current version 29 November 2023.

Digital Object Identifier 10.1109/ACCESS.2023.3335941

RESEARCH ARTICLE

Ergodic Capacity Analysis of Uplink MU-MIMO Systems With Low-Resolution ADCs

YOUYANG XIANG, HANJIE WU, AND XIANTAO CHENG, (Member, IEEE)
National Key Laboratory of Wireless Communications, University of Electronic Science and Technology of China (UESTC), Chengdu 611731, China
Corresponding author: Xiantao Cheng (xiantaocheng@163.com)

This work was supported by the Natural Science Foundation of Sichuan Province under Grant 2022NSFSC0486.

ABSTRACT This paper addresses the ergodic capacity for uplink multi-user multiple-input multiple-output (MU-MIMO) systems equipped with low-resolution analog-to-digital converters (ADCs). The nonlinear quantization effect poses a great challenge to conduct the capacity analysis. This is because the well-known Shannon capacity expression is only applicable for linear systems, and it cannot be directly used for the capacity analysis in the nonlinear quantized systems with low-resolution ADCs. To tackle this, we resort to the replica method from statistical physics. Specifically, we elaborately derive the closed-form expression of the ergodic capacity, which is applicable for arbitrary signaling inputs. As a result, explicit capacity expressions are readily obtained for the often-used Gaussian inputs and QAM inputs. With the obtained expressions, we can evaluate the ergodic capacity for various system setups, and can study the impacts of the system parameters (the number of received antennas, the number of users, the number of quantization bits and the channel parameters) on the ergodic capacity. We directly calculate the mutual information between the transmitted signals and the received quantized signals, without performing any additional reception operations, and obtain more fundamental results. Compared to the time-consuming Monte-Carlo simulations, the analytical expressions are highly accurate while significantly saving the computation time. Furthermore, it is shown that with proper system configurations, the capacity loss caused by low-resolution ADCs may be mild, compared with infinite-precision ADCs.

INDEX TERMS Ergodic capacity, MU-MIMO, low-resolution ADCs, replica method.

I. INTRODUCTION

Due to the ability of supporting many high-data-rate applications, massive multi-user multiple-input multiple-output (MU-MIMO) is a core technology for modern and future wireless communication systems [1], [2], [3], [4]. However, the large number of antennas in MU-MIMO systems dramatically increases the hardware cost and power consumption at the base station (BS), if each antenna bears a pair of high-resolution analog-to-digital converters (ADCs) [5], [6]. Since the power consumption of each ADC exponentially scales with the number of quantization bits Q_b [7], using low-resolution ADCs is regarded as a promising way to alleviate the hardware cost and power consumption issue [8], [9].

The associate editor coordinating the review of this manuscript and approving it for publication was Wei Feng.

The severe nonlinearity introduced by the low-resolution ADCs makes the capacity analysis difficult. Specifically, one cannot rely on the Shannon capacity expression to analyze the capacities of the nonlinear quantized systems with low-resolution ADCs. To bypass this difficulty, researchers often adopt some linear quantization models to approximate the nonlinear quantization operation [10], [11], [12], [13], [14], [15], [16], [17], [18], [19], [20]. With these approximate linear models, the capacity analysis of the quantized systems can be conducted based on the Shannon capacity expression. In [10], [11], [12], [13], [14], and [15], the achievable rate expressions are derived based on the linear additive quantization noise model (AQNM), where the quantization error is modeled as additive Gaussian noise. The results therein reveal that the rate loss caused by low-resolution ADCs can be compensated by using more antennas. In [16], the linear Bussgang's decomposition [21]

is used to approximately model the nonlinear quantization. Based on this, the achievable rate is analyzed. For the mixed-ADC MIMO receiver bearing a small number of high-resolution ADCs but a large number of low-resolution ADCs, the AQNM-based analysis shows that the mixed ADCs can achieve almost the same performance as that of the perfect quantization (corresponding to infinite-precision ADCs) [18], [19], [20]. However, the above studies assume that the quantization process is linear and the signals received at the BS are detected by a non-optimal linear receiver (e.g., maximal ratio combining (MRC) receiver and zero forcing (ZF) receiver). Since the quantization operation is nonlinear in essence, the adoption of the approximate linear quantization models will adversely affect the analysis accuracy. Moreover, due to the data-processing principle [22], the non-optimal linear receiver (i.e., the additional processing of the quantized received signals) will lead to a underestimate of the system capacity.

In this paper, we aim to analyze the ergodic capacity of uplink MU-MIMO systems, where multiple single-antenna users communicate with the BS equipped with N antennas and the BS uses low-resolution ADCs to quantize the received signals. This system setup is similar to that in [10]. However, we will use the accurate nonlinear quantization model, rather than the approximate AQNM used in [10]. Moreover, the analysis in [10] is only applicable for the case where the MRC reception is used to process the received quantized. In contrast, we directly compute the mutual information between the transmitted signals and the received quantized signals, and do not assume any additional receiver operations. Therefore, the derived capacity expressions are more fundamental.

Specifically, the main contributions of our paper can be summarized as follows:

1) By resorting to the replica method from statistical physics [23], [24], [25], [26], [27], [28], [29], [30], [31], we derive the analytical ergodic capacity expression in the large-system regime, i.e., assuming that the number of BS antennas N is very large or goes to infinity. We accurately take into account of the nonlinear quantization effect when conducting the capacity analysis.
2) The derived expression is applicable for arbitrary signaling inputs. In other words, with the obtained expression, one can easily evaluate the ergodic capacity with various signaling inputs. Based on that, for Gaussian inputs and finite-cardinality constellations (i.e., QAM signals), we provide the explicit expressions.
3) For the capacity analysis, we calculate the mutual information between the transmitted signals and the received quantized signals, and do not relay on any additional receiver operations (e.g. MRC data processing of the received signals). Consequently, our capacity results are more fundamental. Due to the data-processing principle [22], the additional MRC processing will lead to a certain information rate loss. In other words, our obtained results embody the system capacity more accurately than those in [10], as will be verified in the simulation section below.
4) Although the capacity expressions are derived in the large-system regime, they are applicable even when the number of BS antennas N is moderate. In other words, the analytical capacity expressions match well with Monte-Carlo simulations when N is not large. Based on this, we can use the analytical expressions, instead of the time-consuming Monte-Carlo simulations, to swiftly investigate the effects of the system parameters (the number of received antennas N, the number of users K, the number of quantization bits Q_b and the channel parameters in (2) in Section II) on the capacity.

The rest of the paper is organized as follows. Section II briefly describes the system model for uplink MU-MIMO with low-resolution ADCs, where the nonlinear quantization operation is accurately characterized. In Section III, we elaborately derive the expression of the ergodic capacity using the replica method, and provide specific capacity expressions for the Gaussian inputs and QAM inputs. In Section IV, simulations are carried out to verify the accuracy of the analytical results. Some insights are gained on the system design. Finally, we draw the conclusions in Section V.

Notation. Lowercase and uppercase boldface letters denote column vector and matrix, respectively. $(\cdot)^R$ and $(\cdot)^I$ denote the real and imaginary parts of a complex-valued argument, respectively. $(\cdot)^T$ and $(\cdot)^H$ denote transpose and Hermitian transpose, respectively. $\mathbf{I}_N$ denotes the identity matrix of size $N \times N$. diag $(\mathbf{a})$ is a diagonal matrix with the vector $\mathbf{a}$ on its diagonal. vec$(\mathbf{A})$ outputs a vector by catenating the columns in the matrix $\mathbf{A}$. a_n denotes the n-th entry of the vector $\mathbf{a}$. $|a|$ denotes the absolute value of the scalar a. det $(\mathbf{A})$ is the determinant of matrix $\mathbf{A}$. $\mathrm{E}_{\mathbf{x}}[f(\mathbf{x})]$ denotes the expectation of $f(\mathbf{x})$ with respect to $\mathbf{x}$. $\mathbf{x} \sim \mathcal{CN}(\boldsymbol{\mu}, \boldsymbol{\Sigma})$ ($x \sim \mathcal{CN}(\mu, \Sigma)$) shows that the vector $\mathbf{x}$ (the scalar x) follows a complex Gaussian distribution with mean vector $\boldsymbol{\mu}$ (mean μ) and covariance matrix $\boldsymbol{\Sigma}$ (variance Σ). $\varphi(x) = \frac{1}{\sqrt{2\pi}} e^{-\frac{x^2}{2}}$ and $\Phi(x) = \int_{-\infty}^{x} \varphi(t)dt$, respectively, represent the probability density function (PDF) and cumulative distribution function (CDF) of a real Gaussian distributed random variable x with zero mean and unit variance. And $Dx = \varphi(x)\,\mathrm{d}x$.

II. UPLINK MU-MIMO SYSTEM MODEL

Consider an uplink MU-MIMO system [10], where K independent single-antenna users communicate with the BS with N receive antennas in the same time-frequency resource, as illustrated in Figure 1. Each BS antenna bears a RF chain, and a pair of low-resolution ADCs, which are used to quantized the real and imaginary parts of the received signal. The baseband quantized received signal $\mathbf{q} \in \mathbb{C}^{N\times 1}$ at the BS

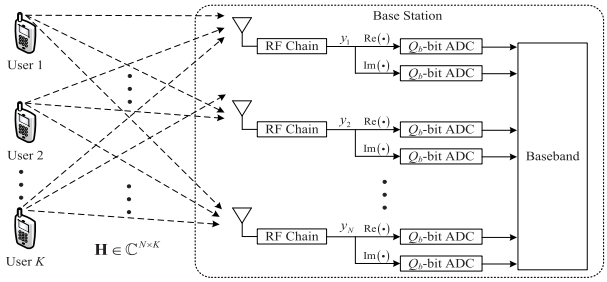

FIGURE 1. The uplink MU-MIMO system model.

can be formulated as

$$\mathbf{q} = \mathcal{Q}_c(\mathbf{y}) = \mathcal{Q}_c(\mathbf{Hs} + \mathbf{n}) = \mathcal{Q}_c\left(\sum_{k=1}^{K} \mathbf{h}_k s_k + \mathbf{n}\right), \quad (1)$$

where $\mathbf{y} \in \mathbb{C}^{N\times 1}$ is the unquatized received signal, $\mathbf{s} = [s_1, s_2, \cdots, s_K]^T \in \mathbb{C}^{K\times 1}$ denotes the transmitted symbol vector of all the K users, s_k is of unit energy and is transmitted from the k-th user, $\mathbf{n} \in \mathbb{C}^{N\times 1}$ is the additive Gaussian white noise (AWGN) with each entry being of zero mean and variance σ^2, $\mathbf{H} = [\mathbf{h}_1, \mathbf{h}_2, \cdots, \mathbf{h}_K] \in \mathbb{C}^{N\times K}$ is the channel matrix, $\mathbf{h}_k \in \mathbb{C}^{N\times 1}$ is the channel vector between the BS and the k-th user, $\mathcal{Q}_c(\cdot)$ represents the complex quantization operation and is applied element-wise. The details of $\mathcal{Q}_c(\cdot)$ will be given later on.

To capture both the small-scale Rayleigh fading and the large-scale fading, the channel matrix $\mathbf{H}$ is modeled as [32]

$$\mathbf{H} = \mathbf{G}\mathbf{D}^{1/2}, \quad (2)$$

where $\mathbf{G} \in \mathbb{C}^{N\times K}$ represents the small-scale fading matrix, the entries in $\mathbf{G}$ are independently and identically distributed as $\mathcal{CN}(0,1)$, $\mathbf{D} = \mathrm{diag}(\beta_1, \beta_2, \cdots, \beta_K) \in \mathbb{C}^{K\times K}$ is a diagonal matrix modeling the large-scale fading, the k-th diagonal entry β_k corresponds to the large-scale fading of the channel between the BS and the k-th user. The large-scale fading coefficients $\{\beta_k\}_{k=1}^K$ characterize the effects of both the geometric attenuation and the shadow fading. With enlarging BS-user distance, the strength of received signals will decrease, leading to the geometric attenuation. On the other hand, the signal strength may vary due to the random blockage between the BS and the users. This effect is referred to as shadow fading. In general, the large-scale fading coefficients are assumed to be constant across the BS antenna array.

Specifically, for the n-th entry of $\mathbf{y}$, the nonlinear quantization operation can be formulated as

$$q_n = \mathcal{Q}_c(y_n) = \mathcal{Q}\left(y_n^R\right) + j\mathcal{Q}\left(y_n^I\right), \quad (3)$$

where y_n^R and y_n^I denote the real and imaginary parts of y_n, respectively, and $\mathcal{Q}(\cdot)$ denotes a conventional real-valued quantizer with Q_b quantization bits. For an arbitrary real-valued scalar y, the quantizer $\mathcal{Q}(\cdot)$ maps it to one of $B = 2^{Q_b}$ discrete values, as shown below

$$\mathcal{Q}(y) = \begin{cases} v_0, & y \in [u_0, u_1], \\ v_1, & y \in (u_1, u_2], \\ \vdots, & \vdots, \\ v_{B-1}, & y \in (u_{B-1}, u_B], \end{cases} \quad (4)$$

where $-\infty = u_0 < u_1 < \cdots < u_B = \infty$ and $v_0 < v_1 < \cdots < v_{B-1}$ are the quantization thresholds and the quantizer output values, respectively. Considering a conventional mid-point uniform quantizer, we have

$$\begin{aligned} u_b &= (-B/2 + b)\,\Delta, \quad b = 1, 2, \cdots, B-1, \\ v_b &= (-(B-1)/2 + b)\,\Delta, \quad b = 0, 1, \cdots, B-1, \end{aligned} \quad (5)$$

where Δ is the quantizer step size, and it can be optimally adjusted to minimize the quantization errors [33].

III. ERGODIC CAPACITY ANALYSIS WITH LOW-RESOLUTION ADCS

The ergodic capacity is defined as the average mutual information between $\mathbf{q}$ and $\mathbf{s}$, as given by

$$\begin{aligned} C &= \mathrm{E}_{\mathbf{H}}[I(\mathbf{q};\mathbf{s} \mid \mathbf{H})] = -\mathrm{E}_{\mathbf{q},\mathbf{H},\mathbf{s}}\left[\log \frac{p(\mathbf{q} \mid \mathbf{H})}{p(\mathbf{q} \mid \mathbf{H}, \mathbf{s})}\right] \\ &= \underbrace{-\mathrm{E}_{\mathbf{q},\mathbf{H}}\left[\log p(\mathbf{q} \mid \mathbf{H})\right]}_{\triangleq H_q} - \underbrace{\left(-\mathrm{E}_{\mathbf{q},\mathbf{H},\mathbf{s}}\left[\log p(\mathbf{q} \mid \mathbf{H}, \mathbf{s})\right]\right)}_{\triangleq H_n}, \end{aligned} \quad (6)$$

where $p(\mathbf{q} \mid \mathbf{H}) = \int_{\mathbf{s}} p(\mathbf{s})\, p(\mathbf{q} \mid \mathbf{H}, \mathbf{s})\, d\mathbf{s}$, $p(\mathbf{s}) = \prod_{k=1}^K p(s_k)$, $p(s_k)$ is the prior distribution of s_k, $p(\mathbf{q} \mid \mathbf{H}, \mathbf{s})$ is the likelihood function, i.e., the distribution of the quantized signal vector $\mathbf{q}$ conditioned on the transmitted vector $\mathbf{s}$ and the channel matrix $\mathbf{H}$.

Specifically, we have $p(\mathbf{q} \mid \mathbf{H}, \mathbf{s}) = p(\mathbf{q} \mid \mathbf{z}) = \prod_{m=0}^{N-1} p(q_m \mid z_m)$, where $\mathbf{z} = \sum_{k=1}^K \mathbf{h}_k s_k$, z_m is the m-th entry of $\mathbf{z}$, and

$$\begin{aligned} &p(q_m \mid z_m) \\ &= \prod_{o\in\{R,I\}} \left[\Phi\left(\frac{\sqrt{2}\left(u_{b+1}^o - z_m^o\right)}{\sigma^2}\right) - \Phi\left(\frac{\sqrt{2}\left(u_b^o - z_m^o\right)}{\sigma^2}\right)\right], \end{aligned} \quad (7)$$

where $q_m^R \in \left[u_b^R, u_{b+1}^R\right]$, $q_m^I \in \left[u_b^I, u_{b+1}^I\right]$, and $\{u_b^R, u_{b+1}^R, u_b^I, u_{b+1}^I\}$ are the quantization thresholds (see (4) and (5)).

Due to the nonlinear quantization effect caused by low-resolution ADCs, it is difficult to calculate the expectations in (6). To address this issue, we are committed to deriving the analytical expression of the ergodic capacity C by using the replica method in the large-system regime [23], [24], [25], [26], [27], [28], [29]. Specifically, we assume that the number of BS antennas goes to infinity, i.e., $N \to \infty$, but the ratio K/N keeps fixed. With this assumption, we can use the replica method to elaborately derive the ergodic capacity.

The obtained expression of the ergodic capacity will be given in Proposition 1 below.

Before presenting Proposition 1, we need to introduce some new parameters for better illustration. These parameters include the mean square error (MSE) and the mutual information metrics corresponding to the following scalar AWGN channels

$$y_{s_k} = \sqrt{\tilde{q}_{s_k}} s_k + n_{s_k},\ k = 1, 2, \cdots, K, \tag{8}$$

where s_k is the transmitted signal (see (1)), $n_{s_k} \sim \mathcal{CN}(0, 1)$ denotes the AWGN, and $\tilde{q}_{s_k}$ denotes the signal-to-noise ratio (SNR) of the k-th AWGN channel. Here it is worthwhile to point out that these scalar AWGN channels are used only to illustrate Proposition 1, and are irrelevant to the system model in Section II. In other words, $\{y_{s_k}, n_{s_k}\}_{k=1}^K$ are irrelevant to $\{\mathbf{y}, \mathbf{n}\}$ in (1).

Based on (8), one can express the Bayesian estimate of s_k as

$$\hat{s}_k = \frac{\int_{s_k} s_k p\left(y_{s_k}|s_k\right) p\left(s_k\right) ds_k}{\int_{s_k} p\left(y_{s_k}|s_k\right) p\left(s_k\right) ds_k}. \tag{9}$$

As a result, the corresponding MSE is given by

$$\mathrm{MSE}_{s_k} = \mathrm{E}_{y_{s_k}, s_k}\left[|s_k - \hat{s}_k|^2\right]. \tag{10}$$

Define the mutual information between y_{s_k} and s_k as

$$\mathcal{I}\left(y_{s_k}; s_k |\sqrt{\tilde{q}_{s_k}}\right) = -\mathrm{E}_{y_{s_k}}\left\{\log \mathrm{E}_{s_k}\left[e^{-\left|y_{s_k} - \sqrt{\tilde{q}_{s_k}} s_k\right|^2}\right]\right\} - 1, \tag{11}$$

then we have [29]

$$\frac{\mathrm{d}}{\mathrm{d}\tilde{q}_{s_k}} I\left(y_{s_k}; s_k \mid \sqrt{\tilde{q}_{s_k}}\right)) = \mathrm{MSE}_{s_k}. \tag{12}$$

With the above preparations, we can clearly express Proposition 1 in the sequel.

Proposition 1: In the large-system regime for the signal model in (1), the ergodic capacity is given by

$$C = \sum_{k=1}^{K}\left[\mathcal{I}\left(y_{s_k}; s_k\right) - \tilde{q}_{s_k}\left(1 - q_{s_k}\right)\right] + 2N\left(\sum_{b=0}^{B-1}\int_z \Omega_{u_b}^{(2)} \log \Omega_{u_b}^{(2)} Dz - \sum_{b=0}^{B-1}\int_z \Omega_{u_b}^{(1)} \log \Omega_{u_b}^{(1)} Dz\right), \tag{13}$$

where $Dz = \varphi(z)\, dz$, $\Omega_{u_b}^{(1)}(z) = \Phi_{u_{b+1}}^{(1)}(z) - \Phi_{u_b}^{(1)}(z)$, $\Omega_{u_b}^{(2)}(z) = \Phi_{u_{b+1}}^{(2)}(z) - \Phi_{u_b}^{(2)}(z)$, and

$$\Phi_{u_b}^{(1)}(z) = \Phi\left(\frac{\sqrt{2}u_b - z\sqrt{\sum_{k=1}^K \beta_k q_{s_k}}}{\chi}\right), \tag{14}$$

$$\Phi_{u_b}^{(2)}(z) = \Phi\left(\frac{\sqrt{2}u_b - z\sqrt{\sum_{k=1}^K \beta_k}}{\sigma}\right), \tag{15}$$

where

$$\chi = \sqrt{\sigma^2 + \sum_{k=1}^K \beta_k\left(1 - q_{s_k}\right)}, \tag{16}$$

and the parameters $\left\{q_{s_k}, \tilde{q}_{s_k}\right\}_{k=1}^K$ are the solutions to the following fixed-point equations

$$\begin{cases} q_{s_k} = 1 - \mathrm{MSE}_{s_k}, \\ \tilde{q}_{s_k} = N\beta_k \sum_{b=0}^{B-1}\int \mathrm{D}z \frac{\left(\varphi_{u_{b+1}}^{(1)}(z) - \varphi_{u_b}^{(1)}(z)\right)^2}{\Omega_{u_b}^{(1)}(z)}, \end{cases} \tag{17}$$

where $k = 1, 2, \cdots, K$, and

$$\varphi_{u_b}^{(1)}(z) = \frac{1}{\chi}\varphi\left(\frac{\sqrt{2}u_b - z\sqrt{\sum_{k=1}^K \beta_k q_{s_k}}}{\chi}\right). \tag{18}$$

Proof: See Appendix.

Here it is worthwhile to provide several remarks:

Remark 1: The results in Proposition 1 can be further extended to the systems with infinite-precision ADCs. As $Q_b \to \infty$, we have

$$\lim_{Q_b\to\infty}\left[\Phi\left(\frac{u_{b+1} - z}{a}\right) - \Phi\left(\frac{u_b - z}{a}\right)\right] = \frac{1}{a}\varphi\left(\frac{u - z}{a}\right) \tag{19}$$

and

$$\lim_{Q_b\to\infty}\left[\varphi\left(\frac{u_{b+1} - z}{a}\right) - \varphi\left(\frac{u_b - z}{a}\right)\right] = \frac{u - z}{a^2}\varphi\left(\frac{u - z}{a}\right). \tag{20}$$

By substituting the above relationships into (13) and (17), we can obtain the ergodic capacity of the systems with infinite-precision ADCs as

$$C_\infty = \sum_{k=1}^K\left[\mathcal{I}\left(y_{s_k}; s_k\right) - \tilde{q}_{s_k}\left(1 - q_{s_k}\right)\right] + N\log\left(1 + \sum_{k=1}^K \frac{\beta_k\left(1 - q_{s_k}\right)}{\sigma^2}\right), \tag{21}$$

where $\left\{q_{s_k}, \tilde{q}_{s_k}\right\}_{k=1}^K$ are the solutions to the following fixed-point equations

$$\begin{cases} q_{s_k} = 1 - \mathrm{MSE}_{s_k}, \\ \tilde{q}_{s_k} = \dfrac{N\beta_k}{\sigma^2 + \sum_{k=1}^K N\beta_k\left(1 - q_{s_k}\right)}. \end{cases} \tag{22}$$

Remark 2: Obviously, the expressions of MSE_{s_k} in (10) and $\mathcal{I}\left(y_{s_k}; s_k\right)$ in (11) depend on the prior of the transmitted symbol s_k. Below we provide two often-used examples for the transmitted symbol s_k:

(1) *Gaussian inputs:* When the transmitted signals follow the Gaussian distribution, i.e., $s_k \sim \mathcal{CN}(0, 1)$, $k =$

TABLE 1. Simulation parameters.

Parameter	Value
Number of users K	4
Number of received antennas N	32
Transmit SNR per user $1/\sigma^2$	$[-10, 50]$ dB
Number of quantization bits Q_b	3 bit
Large-scale fading coefficient β_k	$e_k\,(d_k/d_{\min})^{-\gamma}$
Random shadowing-fading coefficient e_k	Log-normal distribution with $\delta_{\text{shad}} = 6$ dB
Distance between the k-th user and the BS d_k	$\mathcal{U}\,(d_{\min}, d_{\max})$
Minimum BS-user distance $d_{\min}$	100 meters
Maximum BS-user distance $d_{\max}$	1000 meters
Decay exponent γ	1.6

$1, 2, \cdots, K$, the MSE and mutual information are given by

$$\text{MSE}_{s_k} = \frac{1}{1+\tilde{q}_{s_k}}, \tag{23}$$

$$\mathcal{I}\left(y_{s_k}; s_k \mid \sqrt{\tilde{q}_{s_k}}\right) = \log\left(1+\tilde{q}_{s_k}\right). \tag{24}$$

(2) *QAM inputs:* When transmitted signals are drawn from M-QAM constellation, it is hard to obtain the exact analytical expressions of MSE and mutual information. According to [34], an approximate expression of mutual information based on multi-exponential decay curve fitting can be expressed as

$$\mathcal{I}\left(y_{s_k}; s_k \mid \sqrt{\tilde{q}_{s_k}}\right) = \log M\left[1 - \sum_{i=1}^{K_M} a_i^{(M)} e^{-b_i^{(M)}\tilde{q}_{s_k}}\right], \tag{25}$$

where the parameters K_M and $\left\{a_i^{(M)}, b_i^{(M)}, \forall i\right\}$ are given in [34]. Exploiting the relationship between mutual information and MSE in (12), we can obtain

$$\text{MSE}_{s_k} = \log M \sum_{i=1}^{K_M} a_i^{(M)} b_i^{(M)} e^{-b_i^{(M)}\tilde{q}_{s_k}}. \tag{26}$$

IV. SIMULATION AND DISCUSSION

In this section, we conduct simulations to validate the obtained analytical results. The transmit SNR per user is defined as $1/\sigma^2$. If not specified otherwise, the number of users is $K = 4$, the number of received antennas is $N = 32$ and the number of quantization bits is $Q_b = 3$. The large-scale fading coefficient is generated as $\beta_k = e_k\,(d_k/d_{\min})^{-\gamma}$, where e_k is the random log-normal shadowing-fading coefficient, the standard deviation of the log-normal distribution is $\delta_{\text{shad}} = 6$dB, d_k is the distance between the k-th user and the BS, it follows the uniform distribution $d_k \sim \mathcal{U}\,(d_{\min}, d_{\max})$ with $d_{\min} = 100$ meters and $d_{\max} = 1000$ meters being the minimum and maximum BS-user distance respectively, and $\gamma = 1.6$ is the decay exponent. In the following, we will use 'Monte Carlo' and 'Analytical' to represent the results of Monte-Carlo simulations and the analytical results obtained in Section III, respectively. The parameters in the simulation setups are summarized in Table 1.

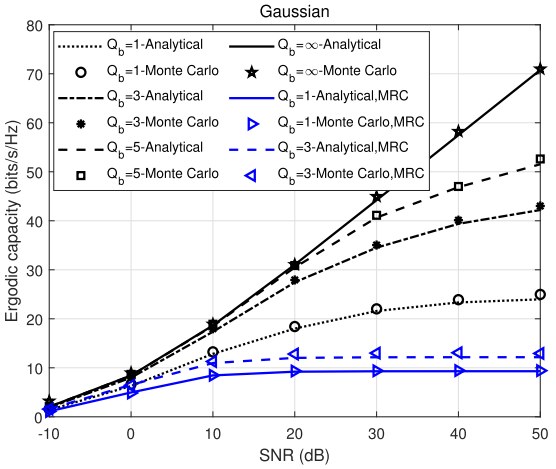

FIGURE 2. The ergodic capacity comparison between the analytical results and the Monte-Carlo simulations for the Gaussian inputs.

With Gaussian inputs, Fig. 2 compares our analytical results with Monte-Carlo simulations, which are conducted according to (6).For comparison, the analytical results and its corresponding Monte-Carlo results in [10] are also presented in Fig. 2. It is noticed that the results in [10] are confined to the MRC reception. Therefore, the analytical results and Monte-Carlo simulations corresponding to [10] are denoted by 'Analytical, MRC' and 'Monte Carlo, MRC', respectively. It can be seen that for various quantization bits Q_b's, our analytical curves merge together with the Monte-Carlo results over a wide range of SNRs, verifying that the analytical expressions are highly accurate. Our results are obtained by directly computing the mutual information between the transmitted signals and the received quantized signals (see (6)), while the results in [10] are based on the use of the MRC receiver to process the received quantized signals. The additional (MRC) processing will underestimate the capacity according to the well-known

TABLE 2. Computation time (seconds) comparison under various system setups.

Inputs	Method	$Q_b = 1$	$Q_b = 3$	$Q_b = 5$	$Q_b = \infty$
Gaussian	Analytical results	0.564926	2.074753	6.926757	0.042222
Gaussian	Monte-Carlo simulations	94.473633	104.111390	111.404366	1.197709
QPSK	Analytical results	0.512269	1.088621	4.261585	0.043542
QPSK	Monte-Carlo simulations	29.139600	29.573018	29.591225	6.059344
16QAM	Analytical results	0.508082	1.771983	6.268365	0.041953
16QAM	Monte-Carlo simulations	5554.012810	6242.861833	6328.718591	959.426243
64QAM	Analytical results	0.548709	1.925223	7.194464	0.043610
64QAM	Monte-Carlo simulations	1941669.641082	2012907.093970	2022642.737610	236876.974092

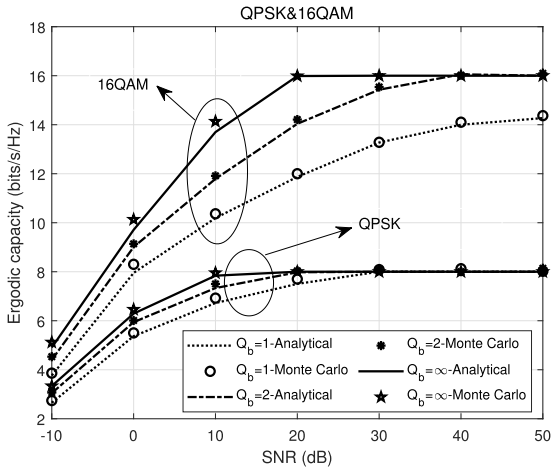

FIGURE 3. The ergodic capacity comparison between the analytical results and the Monte-Carlo simulations for the QPSK inputs and the 16QAM inputs.

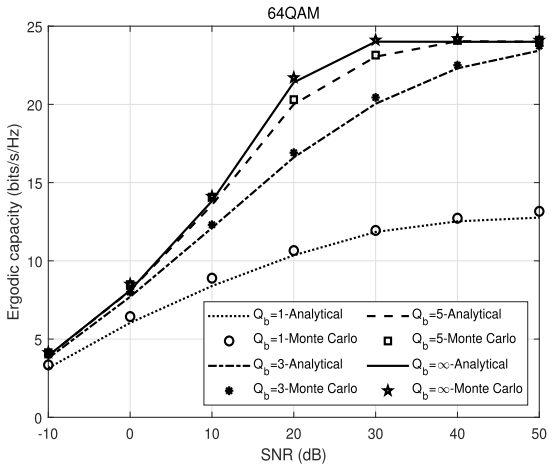

FIGURE 4. The ergodic capacity comparison between the analytical results and the Monte-Carlo simulations for the 64QAM inputs.

data-processing inequality (DPI) in information theory [22]. Therefore, our capacity results are larger than those in [10]. In other words, our analytical capacity results are more fundamental.

In Fig. 3 and Fig. 4, we compare the analytical results with Monte-Carlo simulations for QAM inputs. QPSK and 16QAM are considered in Fig. 3, and 64QAM is considered in Fig. 4. In this case, the capacity analysis in [10] is not applicable any more, since the derivations therein are limited to the Gaussian inputs. As seen from the figures, the analytical results coincide with the Monte-Carlo simulations. This verifies that our analytical expressions are accurately applicable for the QAM inputs. For the QPSK inputs and the 16QAM inputs in Fig. 3, at high SNRs, it is observed that $Q_b = 1$ and $Q_b = 2$ have been able to achieve the ergodic capacity of $Q_b = \infty$, respectively. At the low-to-medium SNRs, $Q_b = 1$ and $Q_b = 2$ can capture a dominant portion of the capacity of $Q_b = \infty$. Therefore, it can be deduced from Fig. 3 that the relatively lower quantization bits (e.g., $Q_b = 1$ and $Q_b = 2$) is sufficient for the QPSK inputs and the 16QAM inputs. For the 64QAM inputs in Fig. 4, we need to increase the number of quantization bits Q_b to improve the performance such that it is as close as possible to that of $Q_b = \infty$. Typically, $Q_b = 3$ and $Q_b = 5$, rather than $Q_b = 1$, are good choices for the 64QAM inputs. The observations in Fig. 3 and Fig. 4 corroborate the feasibility of using low-resolution ADCs in practical MIMO systems, where the finite-cardinality constellations (e.g., QPSK, 16QAM and 64QAM) are widely used. Moreover, for M-QAM inputs, the number of information bits per symbol increases as M increases, thereby resulting in an increase in the capacity. Note that the maximum number of information bits for QPSK, 16QAM and 64QAM are $2, 4$ and 6, respectively. Therefore, with $K = 4$ users, the capacity limits for QPSK, 16QAM and 64QAM are 8, 16 and 24, respectively. In Fig. 3 and Fig. 4, it is observed that the capacity results can converge to the capacity limits, when the SNR and Q_b are sufficiently large. In contrast, there are no capacity limits for Gaussian inputs. With enlarging SNR, the capacity results for Gaussian inputs will continue to increase (if Q_b is not too small), as shown in Fig. 2.

Generally speaking, Monte-Carlo simulations are much higher time-consuming than analytical calculations. This is true for the ergodic capacity problem considered in this paper. To show this, in Table 2 we provide the computation time for

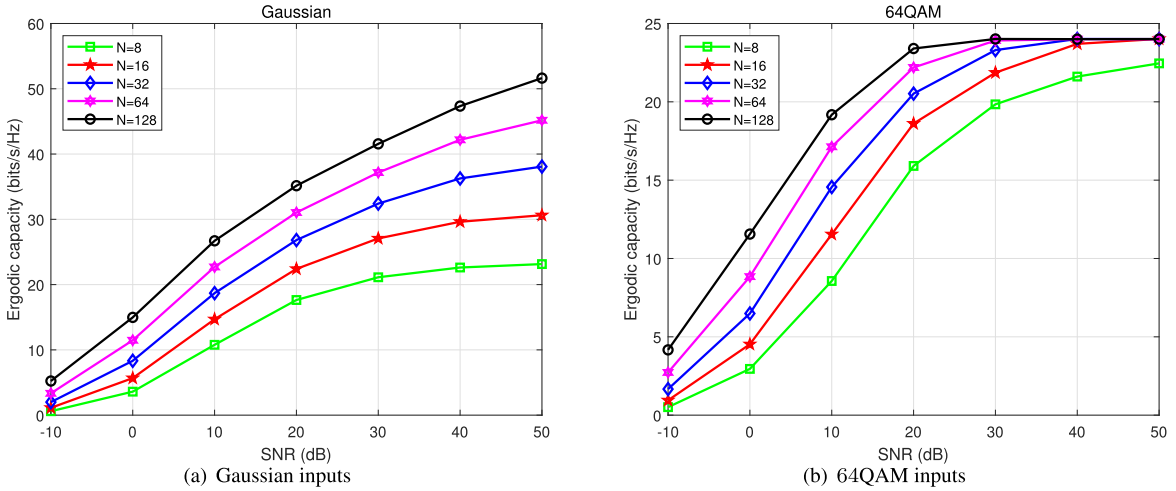

(a) Gaussian inputs (b) 64QAM inputs

FIGURE 5. The ergodic capacity with different number of BS antennas.

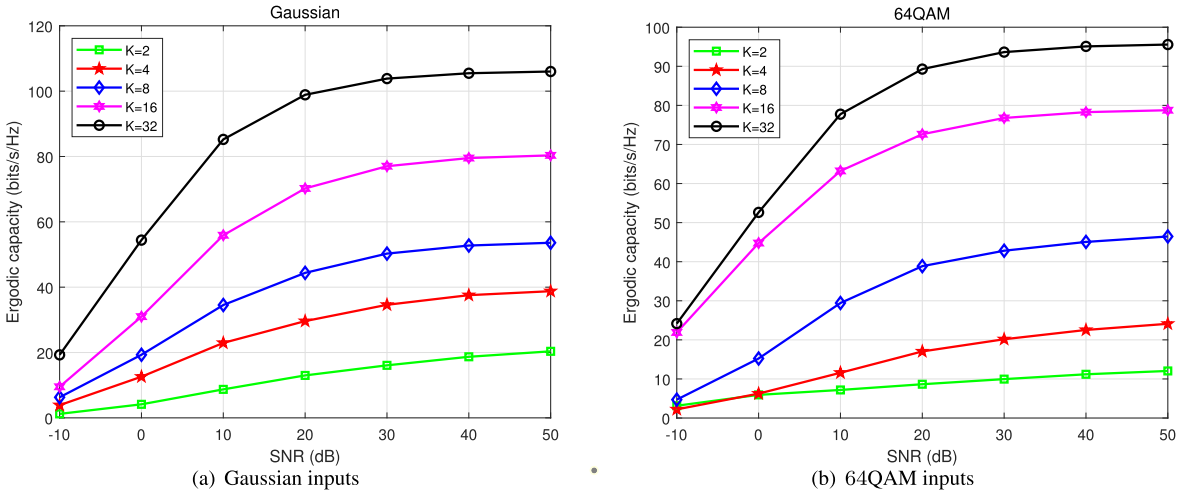

(a) Gaussian inputs (b) 64QAM inputs

FIGURE 6. The ergodic capacity with different number of users.

the Monte-Carlo simulations and the analytical calculations under various system setups. We use a DELL ChengMing 3991 computer to conduct the Monte-Carlo simulations and the analytical calculations. The results in Table 2 correspond to those in Fig. 2–Fig. 4, and are obtained by averaging over the SNR region in Fig. 2–Fig. 4. Obviously, the computation time of calculating the analytical results is several orders of magnitude lower than that of conducting Monte-Carlo simulations. In other words, compared with the analytical calculations, Monte-Carlo simulations are formidably high time-consuming. This is more pronounced for high-order QAM signals. For example, with $Q_b = 3$ and 64QAM inputs, the calculation time differs by 6 orders of magnitude between the analytical calculations and the Monte-Carlo simulations. In short, compared to Monte-Carlo simulations, analytical results can be obtained more easily and quickly. Due to the extremely time-consuming nature of Monte-Carlo simulations, we are inclined to use the analytical expressions for capacity evaluation.

In Fig. 5 and Fig. 6, we investigate the impacts of the number of BS antennas N and the number of users K on the ergodic capacity, where $Q_b = 3$ is used. Specifically, different N's are studied in Fig. 5, and different K's are studied in Fig. 6. The Gaussian inputs are considered in Fig. 5 (a) and Fig. 6 (a), while the 64QAM inputs are considered in Fig. 5 (b) and Fig. 6 (b). With the Gaussian (or 64QAM) inputs, the capacity gradually increases when enlarging N and/or K. Therefore, the overall observations in Fig. 2–Fig. 6 tell that by properly choosing N, K and Q_b, one can compensate the capacity loss caused by low-resolution ADCs.

V. CONCLUSION

This paper addressed the ergodic capacity of uplink MU-MIMO systems with low-resolution ADCs. Unlike the existing works, we took the nonlinear quantization operation into account, leading to a more accurate capacity analysis. By means of the replica method, we derived the general

expression of ergodic capacity, which is applicable for arbitrary signaling inputs. The specific capacity expressions are explicitly provided for the Gaussian inputs and the finite-cardinality constellations, i.e., QAM inputs. Since we directly calculate the mutual information between the transmitted signals and the received quantized signals, and do not perform any additional reception operations, our results are more fundamental. Numerical results confirm that the obtained analytical expressions match well with Monte-Carlo simulations and require much lower computation time. Therefore, one can readily use the analytical expressions to investigate the effects of the system parameters on the capacity. In this way, we can properly design the system to achieve the desired capacity.

APPENDIX
PROOF OF PROPOSITION 1

According to (6), the computation of the ergodic capacity can be decomposed as the computations of H_q and H_n. In the following, we are committed to computing the detailed expressions of H_q and H_n by using the replica method [23], [24], [25], [26], [27], [28], [29].

(1) *Computing H_q:* Define

$$\mathcal{F} = \lim_{N\to\infty} H_q = -\lim_{N\to\infty} \mathrm{E}_{\mathbf{q},\mathbf{H}}\left[\log p\left(\mathbf{q} \mid \mathbf{H}\right)\right]. \tag{27}$$

To facilitate the derivation, we use the equation [24]

$$\mathbb{E}\left[\log A\right] = \lim_{\tau\to 0} \frac{\partial}{\partial \tau} \log \mathbb{E}\left[\log A^{\tau}\right] \tag{28}$$

and rewrite $\mathcal{F}$ as

$$\mathcal{F} = -\lim_{N\to\infty}\lim_{\tau\to 0} \frac{\partial}{\partial \tau} \log \mathrm{E}_{\mathbf{q},\mathbf{H}}\left[p^{\tau}\left(\mathbf{q} \mid \mathbf{H}\right)\right]. \tag{29}$$

where we assume that the order of the two limits $N \to \infty$ and $\tau \to 0$ can be interchanged [24].

Furthermore, we use the following two assumptions [24]: (1) The obtained $\mathcal{F}$ is applicable for arbitrary τ. (2) τ is an integer. In this way, $\mathrm{E}_{\mathbf{q},\mathbf{H}}\left[p^{\tau}\left(\mathbf{q} \mid \mathbf{H}\right)\right]$ in (29) can be expressed as

$$\begin{aligned}\mathrm{E}_{\mathbf{q},\mathbf{H}}\left[p^{\tau}\left(\mathbf{q} \mid \mathbf{H}\right)\right] &= \mathrm{E}_{\mathbf{q},\mathbf{H}}\left\{\mathrm{E}_{\mathbf{s}}^{\tau}\left[p\left(\mathbf{q} \mid \mathbf{H}, \mathbf{s}\right)\right]\right\} \\ &= \mathrm{E}_{\mathcal{E}_s}\left\{\int \mathrm{E}_{\mathbf{H}}\left[\prod_{a=0}^{\tau} p\left(\mathbf{q} \mid \mathbf{H}, \mathbf{s}^{(a)}\right)\right] d\mathbf{q}\right\} \\ &= \int \mathrm{E}_{\mathcal{Z}}\left[\prod_{a=0}^{\tau} p\left(\mathbf{q} \mid \mathbf{z}^{(a)}\right)\right] d\mathbf{q}, \end{aligned} \tag{30}$$

where $\mathcal{E}_s \triangleq \{\mathbf{s}_k\}_{k=1}^{K}$, $\mathbf{s}_k \triangleq \left[s_k^{(0)}, s_k^{(1)}, \cdots, s_k^{(\tau)}\right]$, $s_k^{(a)}$ is the a-th replica of s_k, $\mathbf{z}^{(a)} = \sum_{k=1}^{K} \mathbf{z}_k^{(a)}$, $\mathcal{Z} = \{\mathbf{Z}_k\}_{k=1}^{K}$, $\mathbf{Z}_k \triangleq \left[\mathbf{z}_k^{(0)}, \mathbf{z}_k^{(1)}, \cdots, \mathbf{z}_k^{(\tau)}\right]$, and $\mathbf{z}_k^{(a)} = \mathbf{h}_k s_k^{(a)}$ for all k and a.

To compute the expectation w.r.t. $\mathcal{E}_s$ in (30), we introduce a set of $(\tau+1)\times(\tau+1)$ matrices $\left\{\mathbf{Q}_{s_k}\right\}_{k=1}^{K}$ and the (a,b)-th entry of $\mathbf{Q}_{s_k}$ is defined by $Q_{s_k}^{ab} \triangleq \left(s_k^{(a)}\right)^{*} s_k^{(b)}$. The above definition is equivalent to

$$1 = \int \prod_{0\le a\le b}^{\tau} \delta\left(\left(s_k^{(a)}\right)^{*} s_k^{(b)} - Q_{s_k}^{ab}\right) dQ_{s_k}^{ab}, \tag{31}$$

where $\delta(\cdot)$ denotes Dirac delta function. By using the results in [27], we arrive at

$$\mathrm{E}_{\mathbf{q},\mathbf{H}}\left[p^{\tau}\left(\mathbf{q} \mid \mathbf{H}\right)\right] = \int e^{M^{(\tau)}(\mathcal{Q}_z)} d\mu_s^{(\tau)}\left(\mathbf{Q}_s\right) + \mathcal{O}\left(1\right), \tag{32}$$

where $\mathcal{O}(\cdot)$ is Big-O notation, and

$$M^{(\tau)}\left(\mathcal{Q}_z\right) \triangleq \log \mathrm{E}_{\mathcal{Z}}\left[\int \prod_{a=0}^{\tau} p\left(\mathbf{q} \mid \mathbf{z}^{(a)}\right) d\mathbf{q}\right], \tag{33}$$

$$\mu_s^{(\tau)}\left(\mathbf{Q}_s\right) = \mathrm{E}_{\mathcal{E}_s}\left[\int \prod_{k=1}^{K}\prod_{0\le a\le b}^{\tau} \delta\left(\left(s_k^{(a)}\right)^{*} s_k^{(b)} - Q_{s_k}^{ab}\right)\right], \tag{34}$$

where $\mathcal{Q}_z = \left\{\mathbf{Q}_{z_0}, \cdots, \mathbf{Q}_{z_{N-1}}\right\}$, $\mathbf{Q}_{z_n} \in \mathbb{R}^{(\tau+1)\times(\tau+1)}$ is the covariance matrix of $\mathbf{z}_n \triangleq \left[z_n^{(0)}, z_n^{(1)}, \cdots, z_n^{(\tau)}\right]^{T}$, the (a,b)-th entry of $\mathbf{Q}_{z_n}$ is $Q_{z_n}^{ab} = \mathrm{E}_{\mathbf{h}_n}\left[\left(z_n^{(a)}\right)^{*}\left(z_n^{(b)}\right)\right]$, and $\mathbf{Q}_s = \left\{\mathbf{Q}_{s_k}\right\}_{k=1}^{K}$.

Define

$$\mathcal{F}^{(\tau)} \triangleq -\lim_{N\to\infty} \log \mathrm{E}_{\mathbf{q},\mathbf{H}}\left[p^{\tau}\left(\mathbf{q} \mid \mathbf{H}\right)\right]. \tag{35}$$

Then we can first compute $\mathcal{F}^{(\tau)}$, and subsequently derive $\mathcal{F}$ by using $\mathcal{F} = \lim_{\tau\to 0} \frac{\partial \mathcal{F}^{(\tau)}}{\partial \tau}$. Following the results in [25], the expression of $\mathcal{F}^{(\tau)}$ is given by

$$\mathcal{F}^{(\tau)} = -\underset{\mathbf{Q}_s}{\mathrm{Extr}}\left\{M^{(\tau)}(\mathcal{Q}_z) - \sum_{k=1}^{K} \mathcal{R}_{s_k}^{(\tau)}(\mathbf{Q}_{s_k})\right\}, \tag{36}$$

where $\mathrm{Extr}\{\cdot\}$ denotes the extreme operation, and

$$\mathcal{R}_{s_k}^{(\tau)}(\mathbf{Q}_{s_k}) = \max_{\tilde{\mathbf{Q}}_{s_k}}\left\{\mathrm{tr}\left(\tilde{\mathbf{Q}}_{s_k}\mathbf{Q}_{s_k}\right) - \log \mathrm{E}_{\mathbf{s}_k}\left(e^{\mathrm{tr}\left(\tilde{\mathbf{Q}}_{s_k}\mathbf{s}_k^{H}\mathbf{s}_k\right)}\right)\right\}. \tag{37}$$

Therefore, the computation of $\mathcal{F}^{(\tau)}$ can be decomposed as the computations of (33) and (37). Based on replica symmetry [24], we assume that

$$\mathbf{Q}_{s_k} = \left(c_{s_k} - q_{s_k}\right)\mathbf{I}_{\tau+1} + q_{s_k}\mathbf{I}_{\tau+1}^{(1)}, \tag{38}$$

$$\tilde{\mathbf{Q}}_{s_k} = \left(\tilde{c}_{s_k} - \tilde{q}_{s_k}\right)\mathbf{I}_{\tau+1} + \tilde{q}_{s_k}\mathbf{I}_{\tau+1}^{(1)}, \tag{39}$$

where $\mathbf{I}_{\tau+1}^{(1)}$ is the matrix with all entries equal to 1. Then $Q_{z_n}^{ab}$ can be expressed as $Q_{z_n}^{ab} = \sum_{k=1}^{K} \beta_k Q_{s_k}^{ab}$. Besides, we denote the n-th entry of $\mathbf{z}^{(a)}$ by $z_n^{(a)}$. Obviously, $z_n^{(a)}$ is a Gaussian random variable. Thus we can introduce two independent standard complex Gaussian random variables v_c and $u_c^{(a)}$ to represent $z_n^{(a)}$ as

$$z_n^{(a)} = v_c\sqrt{\sum_{k=1}^{K}\beta_k q_{s_k}} + u_c^{(a)}\sqrt{\sum_{k=1}^{K}\beta_k\left(c_{s_k} - q_{s_k}\right)}. \tag{40}$$

We substitute (40) into (33) and perform the expectation w.r.t. $\mathcal{Z}$ and the integral over $\mathbf{q}$ to yield

$$M^{(\tau)}(\mathcal{Q}_z) = 2N \log\left(\sum_{b=0}^{B-1} \int \left[\Omega_{u_b}^{(1)}(z)\right]^{\tau+1} Dz\right). \quad (41)$$

Moreover, after using the Hubbard-Stratonovich transformation and performing some straightforward operations, we get

$$\mathcal{R}_{s_k}^{(\tau)}(\mathbf{Q}_{s_k}) = \max_{\tilde{c}_{s_k}, \tilde{q}_{e_k}} \left\{\left[(\tau+1)\,\tilde{c}_{s_k} c_{s_k} + (\tau+1)\,\tau \tilde{q}_{s_k} q_{s_k} - \log \mathcal{M}_{s_k}^{(\tau)}\right]\right\}, \quad (42)$$

where

$$\mathcal{M}_{s_k}^{(\tau)} = \mathrm{E}_{s_k}\left\{\int \mathrm{d}y_{s_k} \frac{1}{\pi} e^{-\left|y_{s_k} - \sqrt{\tilde{q}_{s_k}} s_k\right|^2 + \tilde{c}_{s_k} s_k^* s_k}\right\} \times \left(\mathrm{E}_{s_k}\left\{e^{\left(\sqrt{\tilde{q}_{s_k}} s_k\right)^* y_{s_k} + y_{s_k}^* \left(\sqrt{\tilde{q}_{s_k}} s_k\right) + (\tilde{c}_{s_k} - \tilde{q}_{s_k}) s_k^* s_k}\right\}\right)^{\tau}. \quad (43)$$

Plugging (41) and (42) into (36), we can get $\mathcal{F}^{(\tau)}$. With the normalization constraint $\lim_{\tau\to 0} \mathrm{E}_{\mathbf{q}}\left[p^{\tau}(\mathbf{q})\right] = 1$, we set the partial derivatives of $\mathcal{F}^{(\tau)}$ w.r.t. $\{c_{s_k}\}_{k=1}^K$ and $\{\tilde{c}_{s_k}\}_{k=1}^K$ to zero and then have $c_{s_k} = \mathrm{E}\left[|s_k|^2\right] = 1$ and $\tilde{c}_{s_k} = 0$. By using $\mathcal{F} = \lim_{\tau\to 0} \frac{\partial \mathcal{F}^{(\tau)}}{\partial \tau}$, we obtain the free entropy $\mathcal{F}$. Equating the partial derivatives of $\mathcal{F}$ w.r.t. $\{q_{s_k}\}_{k=1}^K$ and $\{\tilde{q}_{s_k}\}_{k=1}^K$ to zero, we arrive at the fixed-point equations given in (17).

(2) *Computing H_n:* Since $\{\mathbf{h}_k\}_{k=1}^K$ are Gaussian distributed vectors, $\mathbf{z}$ follows a complex Gaussian distribution with mean vector $\mathbf{0}$ and covariance matrix $\left(\sum_{k=1}^K \beta_k\right)\mathbf{I}_N$. The expectation for $\mathbf{H}$ and $\mathbf{s}$ in H_n can be transformed into expectation for $\mathbf{z}$, and then the high dimensional integrals in H_n are reduced to B one-dimension integrals. Thus we have

$$H_n = -2N\left(\sum_{b=0}^{B-1} \int_z \Omega_{u_b}^{(2)} \log \Omega_{u_b}^{(2)} Dz\right). \quad (44)$$

With the above derived expressions of H_q and H_n, we can get the capacity C in (13).

REFERENCES

[1] J. G. Andrews, S. Buzzi, W. Choi, S. V. Hanly, A. Lozano, A. C. K. Soong, and J. C. Zhang, "What will 5G be?" *IEEE J. Sel. Areas Commun.*, vol. 32, no. 6, pp. 1065–1082, Jun. 2014.

[2] C.-X. Wang, F. Haider, X. Gao, X.-H. You, Y. Yang, D. Yuan, H. M. Aggoune, H. Haas, S. Fletcher, and E. Hepsaydir, "Cellular architecture and key technologies for 5G wireless communication networks," *IEEE Commun. Mag.*, vol. 52, no. 2, pp. 122–130, Feb. 2014.

[3] T. L. Marzetta and Y. Hong, *Fundamentals of Massive MIMO*. Cambridge, U.K.: Cambridge Univ. Press, 2016.

[4] V. W. Wong, R. Schober, D. W. K. Ng, and L. C. Wang, *Key Technologies for 5GWireless Systems*. Cambridge, U.K.: Cambridge Univ. Press, 2017.

[5] T. L. Marzetta, "Noncooperative cellular wireless with unlimited numbers of base station antennas," *IEEE Trans. Wireless Commun.*, vol. 9, no. 11, pp. 3590–3600, Nov. 2010.

[6] H. Q. Ngo, E. G. Larsson, and T. L. Marzetta, "Energy and spectral efficiency of very large multiuser MIMO systems," *IEEE Trans. Commun.*, vol. 61, no. 4, pp. 1436–1449, Apr. 2013.

[7] H.-S. Lee and C. G. Sodini, "Analog-to-digital converters: Digitizing the analog world," *Proc. IEEE*, vol. 96, no. 2, pp. 323–334, Feb. 2008.

[8] J. Zhang, L. Dai, Z. He, S. Jin, and X. Li, "Performance analysis of mixed-ADC massive MIMO systems over Rician fading channels," *IEEE J. Sel. Areas Commun.*, vol. 35, no. 6, pp. 1327–1338, Jun. 2017.

[9] J. Mo, A. Alkhateeb, S. Abu-Surra, and R. W. Heath, "Hybrid architectures with few-bit ADC receivers: Achievable rates and energy-rate tradeoffs," *IEEE Trans. Wireless Commun.*, vol. 16, no. 4, pp. 2274–2287, Apr. 2017.

[10] L. Fan, S. Jin, C.-K. Wen, and H. Zhang, "Uplink achievable rate for massive MIMO systems with low-resolution ADC," *IEEE Commun. Lett.*, vol. 19, no. 12, pp. 2186–2189, Dec. 2015.

[11] J. Zhang, L. Dai, S. Sun, and Z. Wang, "On the spectral efficiency of massive MIMO systems with low-resolution ADCs," *IEEE Commun. Lett.*, vol. 20, no. 5, pp. 842–845, May 2016.

[12] Y. Dong and L. Qiu, "Spectral efficiency of massive MIMO systems with low-resolution ADCs and MMSE receiver," *IEEE Commun. Lett.*, vol. 21, no. 8, pp. 1771–1774, Aug. 2017.

[13] B. D. Antwi-Boasiako, R. K. Ahiadormey, P. Anokye, and K.-J. Lee, "On the performance of massive MIMO full-duplex relaying with low-resolution ADCs," *IEEE Commun. Lett.*, vol. 26, no. 6, pp. 1259–1263, Jun. 2022.

[14] Y. Xiong, S. Sun, L. Liu, S. Mao, Z. Zhang, and N. Wei, "Performance analysis of cell-free massive MIMO network with large-scale-fading decoding and low-resolution ADCs," *IEEE Trans. Veh. Technol.*, vol. 72, no. 10, pp. 13723–13728, May 2023.

[15] P. Anokye, D. K. P. Asiedu, and K.-J. Lee, "Power optimization of cell-free massive MIMO with full-duplex and low-resolution ADCs," *IEEE Trans. Wireless Commun.*, vol. 22, no. 10, pp. 6706–6723, Oct. 2023.

[16] S. Jacobsson, G. Durisi, M. Coldrey, U. Gustavsson, and C. Studer, "Throughput analysis of massive MIMO uplink with low-resolution ADCs," *IEEE Trans. Wireless Commun.*, vol. 16, no. 6, pp. 4038–4051, Jun. 2017.

[17] N. Liang and W. Zhang, "Mixed-ADC massive MIMO uplink in frequency-selective channels," *IEEE Trans. Commun.*, vol. 64, no. 11, pp. 4652–4666, Nov. 2016.

[18] W. Tan, S. Jin, C.-K. Wen, and Y. Jing, "Spectral efficiency of mixed-ADC receivers for massive MIMO systems," *IEEE Access*, vol. 4, pp. 7841–7846, 2016.

[19] Q. Ding and Y. Jing, "Receiver energy efficiency and resolution profile design for massive MIMO uplink with mixed ADC," *IEEE Trans. Veh. Technol.*, vol. 67, no. 2, pp. 1840–1844, Feb. 2018.

[20] Z. Liu, J. Zhang, Z. Wang, X. Zhang, H. Xiao, and B. Ai, "Cell-free massive MIMO with mixed-resolution ADCs and I/Q imbalance over Rician spatially correlated channels," *IEEE Trans. Veh. Tech.*, vol. 72, no. 7, pp. 9567–9572, Jul. 2023.

[21] J. J. Bussgang, *Crosscorrelation Functions of Amplitude Distorted Gaussian Signals*. Cambridge, MA, USA: Massachusetts Institute of Technology, 1952.

[22] M. Thomas and A. T. Joy, *Elements of Information Theory*. Hoboken, NJ, USA: Wiley-Interscience, 2006.

[23] H. Nishimori, *Statistical Physics of Spin Glasses and Information Processing: An Introduction*. Oxford, U.K.: Oxford Univ. Press, 2001.

[24] T. Tanaka, "A statistical-mechanics approach to large-system analysis of CDMA multiuser detectors," *IEEE Trans. Inf. Theory*, vol. 48, no. 11, pp. 2888–2910, Nov. 2002.

[25] C.-K. Wen, C.-J. Wang, S. Jin, K.-K. Wong, and P. Ting, "Bayes-optimal joint channel-and-data estimation for massive MIMO with low-precision ADCs," *IEEE Trans. Signal Process.*, vol. 64, no. 10, pp. 2541–2556, May 2016.

[26] H. Wang, C.-K. Wen, and S. Jin, "Bayesian optimal data detector for mmWave OFDM system with low-resolution ADC," *IEEE J. Sel. Areas Commun.*, vol. 35, no. 9, pp. 1962–1979, Sep. 2017.

[27] Y. Kabashima, F. Krzakala, M. Mézard, A. Sakata, and L. Zdeborová, "Phase transitions and sample complexity in Bayes-optimal matrix factorization," *IEEE Trans. Inf. Theory*, vol. 62, no. 7, pp. 4228–4265, Jul. 2016.

[28] D. Guo, S. Shamai, and S. Verdu, "Mutual information and minimum mean-square error in Gaussian channels," *IEEE Trans. Inf. Theory*, vol. 51, no. 4, pp. 1261–1282, Apr. 2005.

[29] D. Guo and S. Verdu, "Randomly spread CDMA: Asymptotics via statistical physics," *IEEE Trans. Inf. Theory*, vol. 51, no. 6, pp. 1983–2010, Jun. 2005.

[30] K. Xu, J. Zhang, X. Yang, S. Ma, and G. Yang, "On the sum-rate of RIS-assisted MIMO multiple-access channels over spatially correlated Rician fading," *IEEE Trans. Commun.*, vol. 69, no. 12, pp. 8228–8241, Dec. 2021.
[31] J. Zhang, J. Liu, S. Ma, C.-K. Wen, and S. Jin, "Large system achievable rate analysis of RIS-assisted MIMO wireless communication with statistical CSIT," *IEEE Trans. Wireless Commun.*, vol. 20, no. 9, pp. 5572–5585, Sep. 2021.
[32] S. Ghacham, M. Benjillali, L. Van der Perre, and Z. Guennoun, "Rate analysis of uplink massive MIMO with low-resolution ADCs and ZF detectors over Rician fading channels," *IEEE Commun. Lett.*, vol. 23, no. 9, pp. 1631–1635, Sep. 2019.
[33] H. Wang, W.-T. Shih, C.-K. Wen, and S. Jin, "Reliable OFDM receiver with ultra-low resolution ADC," *IEEE Trans. Commun.*, vol. 67, no. 5, pp. 3566–3579, May 2019.
[34] C. Ouyang, S. Wu, C. Jiang, D. W. K. Ng, and H. Yang, "Receive antenna selection under discrete inputs: Approximation and applications," *IEEE Trans. Commun.*, vol. 68, no. 4, pp. 2634–2647, Apr. 2020.

YOUYANG XIANG received the B.S. degree from Harbin Engineering University (HEU), Harbin, China, in 2020, and the M.S. degree from the University of Electronic Science and Technology of China (UESTC), Chengdu, China, in 2023. His current research interests include wireless communications and compressive sensing (CS).

HANJIE WU received the B.S. degree from Harbin Engineering University (HEU), Harbin, China, in 2022. She is currently pursuing the M.S. degree with the University of Electronic Science and Technology of China (UESTC), Chengdu, China. Her current research interests include wireless communications and multi-IRS-assisted mmWave MIMO communication.

XIANTAO CHENG (Member, IEEE) received the B.S. and M.S. degrees from Harbin Engineering University (HEU), Harbin, China, in 1998 and 2001, respectively, and the Ph.D. degree from the University of Electronic Science and Technology of China (UESTC), Chengdu, China, in 2006.

From November 2006 to April 2009, he conducted research with the School of Electrical and Electronic Engineering, Nanyang Technological University, Singapore, with a focus on UWB communications. Since May 2009, he has been with the National Key Laboratory of Wireless Communications, UESTC. His current research interests include millimeter-wave/THz communications (MWC), MIMO techniques, compressive sensing (CS), and machine learning.